

Joint Hyperspectral Superresolution and Unmixing With Interactive Feedback

Chen Yi, Yong-Qiang Zhao, *Member, IEEE*, Jingxiang Yang, *Student Member, IEEE*, Jonathan Cheung-Wai Chan, and Seong G. Kong, *Senior Member, IEEE*

Abstract—This paper presents an interactive feedback scheme of spatial resolution enhancement and spectral unmixing in hyperspectral imaging. Traditionally spatial resolution enhancement and spectral unmixing operations have been carried out separately, often in series. In such sequential processing, spatially enhanced hyperspectral images (HSIs) may introduce distortion in spectral fidelity making spectral unmixing results unreliable, or vice versa. Since both high- and low-resolution HSIs have the same endmembers, the deviation in spectral unmixing between targets and estimated high-resolution HSIs can be used as feedback to control spatial resolution enhancement. The spatial difference before and after unmixing can also be used as feedback to enhance spectral unmixing. Therefore, spectral unmixing is utilized as a constraint to spatial resolution enhancement, while spatial resolution enhancement helps improve spectral unmixing results. The performance of spatial resolution enhancement and spectral unmixing can be improved since one behaves like a prior to the other. Experimental results on both simulated and real HSI data sets demonstrate that the proposed interactive feedback scheme simultaneously achieved spatial resolution enhancement and spectral unmixing fidelity. This paper is an extended version of the previous work.

Index Terms—Hyperspectral image (HSI), interactive feedback, sparsity, spectral unmixing, superresolution enhancement.

I. INTRODUCTION

HYPERSPECTRAL imaging techniques collect images of a scene in tens to hundreds of contiguous narrow spectral

Manuscript received April 6, 2016; revised September 19, 2016 and December 9, 2016; accepted February 8, 2017. Date of publication April 6, 2017; date of current version June 22, 2017. This work was supported in part by the National Natural Science Foundation of China under Grant 61371152, Grant 61071172, and Grant 61374162, in part by the National Natural Science Foundation of China and South Korean National Research Foundation Joint Funded Cooperation Program under Grant 61511140292, in part by the New Century Excellent Talents Award Program from the Ministry of Education of China under Grant NCET-12-0464, in part by the Ministry of Education Scientific Research Foundation for the Returned Overseas, in part by the Fundamental Research Funds for the Central Universities under Grant 3102015ZY045, in part by the China Scholarship Council for joint Ph.D. students under Grant 201506290120, and in part by the Innovation Foundation of Doctor Dissertation of Northwestern Polytechnical University under Grant CX201621. (Corresponding author: Yong-Qiang Zhao.)

C. Yi, Y.-Q. Zhao, and J. Yang are with the Key Laboratory of Information Fusion Technology, Ministry of Education of China, School of Automation, Northwestern Polytechnical University, Xi'an 710072, China (e-mail: chenyi0818@mail.nwp.edu.cn; zhaoyq@nwp.edu.cn; yang123jx@mail.nwp.edu.cn).

J. C.-W. Chan is with the Department of Electronics and Informatics, Vrije Universiteit Brussel, 1050 Brussel, Belgium (e-mail: jchewg@etro.vub.ac.be).

S. G. Kong is with the Department of Computer Engineering, Sejong University, Seoul 05006, South Korea (e-mail: skong@sejong.edu).

Color versions of one or more of the figures in this paper are available online at <http://ieeexplore.ieee.org>.

Digital Object Identifier 10.1109/TGRS.2017.2681721

bands, often in the range from the visible to the infrared region of the electromagnetic spectrum [2]–[5]. Abundant spatial and spectral information contained in hyperspectral images (HSIs) enable discrimination of various materials of an object in observed scenes in many applications such as environmental monitoring, target detection, quality assessment, and military surveillance [6]–[9]. However, factors like imperfect imaging optics, atmospheric scattering, and sensor noise can have negative influences on the integrity of acquired data making subsequent processing and interpretation tasks more challenging. Wide band coverage of hyperspectral sensors often lead to low spatial resolution since the difference in spatial resolution comes as a result of fundamental tradeoff between spatial and spectral resolution in the design of electro-optical sensor systems. Denoising and superresolution enhancement have been suggested as a cost-effective means to obtain higher quality HSIs rather than improving imaging optics or sensor arrays [10], [11].

Spatial resolution enhancement attempts to reconstruct higher resolution HSIs from their lower resolution data. Approaches in the frequency domain include the discrete Fourier transform method [12] and the wavelet transform method [13]. Superresolution methods in spatial domain such as the iterative back projection (IBP) [14] and the projection onto convex sets (POCS) [15] methods provide flexibility in modeling noise and degradation. In superresolution enhancement of HSIs, a band-by-band enhancement approach may not be preferred because of low correlation among spectral bands and huge computational burden [16]. In terms of information resource, recent hyperspectral superresolution enhancement approaches can be classified into three categories: panchromatic and HSI, multispectral and HSI, and multiangular HSI. The fusion of panchromatic and HSIs refers to hyperspectral pan sharpening that includes Principal Component Analysis (PCA) [17], intensity-hue-saturation [18], multiscale analysis method [19], and dictionary-based method [20], [21]. Despite high spatial resolution results, such classical approaches may experience serious spectral distortions. Dictionary-based methods employ coupled dictionaries [22] or semicoupled dictionaries [23]. While Zhu and Bamler [21] reconstructed high-resolution data based on high-/low-dictionary pairs extracted from a panchromatic image and its degraded version, Zhao *et al.* [20] utilized dictionary training using both panchromatic images and HSIs. Fusion of multispectral image and HSI can be achieved through different approaches, such as wavelet transform [24], spatially varying statistical-based model [25],

dictionary learning [26], and unmixing-based methods [27]. Spectral unmixing estimates fractional abundances of pure spectral signatures (endmembers) in each mixed pixel of an HSI in remote sensing. For example, Yokoya *et al.* [27] obtained high spectral resolution endmembers and high spatial resolution abundance maps, respectively, from HSI and multispectral images to reconstruct high spatial resolution results with higher spectral consistency and less spectral distortions. Superresolution methods of multiangular HSI acquired by a specific satellite, such as the Compact High Resolution Image Spectrometer/Project for On-Board Autonomy are summarized in [14], where superresolution methods POCS, IBP, and l_1 norm total variation are demonstrated.

Attempts to improve the resolution in spatial domain only may destroy the correlation among spectral bands that can result in spectral distortion or artifacts. Spectral unmixing can be exploited as a constraint to solve this problem. Every pixel in an HSI can be separated by endmembers into a set of fraction abundances, assumed to represent percentage of pure materials in the pixel [28]. For any given scene, one spectral unmixing abundance map is generated corresponding to one specific spatial resolution. When the spatial resolution is enhanced, its corresponding spectral abundance map will change, but with fixed endmembers [20]. Whatever the spatial resolution is, the endmembers in observed scene does not change [2]. Conventionally, spatial superresolution enhancement and spectral unmixing are implemented separately, in series, which inevitably suffer from spatial and spectral defects such as spectral distortions and inaccurate located endmembers, making it difficult to eliminate or suppress those artifacts. Negative effects of the artifacts are prone to accumulate in sequential processing steps.

This paper presents an HSI spatial resolution enhancement algorithm based on interactive feedback between spatial superresolution enhancement and spectral unmixing. Endmembers are assumed to be the same before and after spatial enhancement, while the high and low abundances obey the spatial degradation relationship. Spectral priors provided by unmixing are used as regularizations in spatial enhancement. And the spatial difference before and after spectral unmixing plays a role as feedback to control spectral unmixing. The endmembers and their abundances are employed to reduce spectral distortions in the superresolution enhancement step. Higher spatial resolution is exploited to acquire more accurate spectral information. Since the two procedures alternatively regularize each other, the proposed interactive feedback framework achieves higher performance and robustness of spatial superresolution and spectral unmixing.

The remainder of this paper is organized as follows. In Section II, the relationship of spatial resolution enhancement and spectral unmixing are analyzed based on a sparse spatial superresolution model and a linear unmixing model. Section III shows the core idea of the joint framework in detail and demonstrates the benefits. The process and the solver of joint hyperspectral superresolution and unmixing (JHSr-Un) algorithm are also described. Experiments as well as the analyses on simulated and real data sets are presented in Section IV. Section V draws a conclusion.

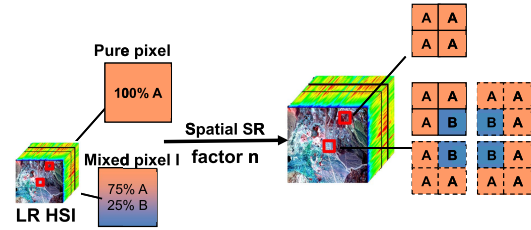


Fig. 1. Spatial resolution enhancement reduces the amount of mixed pixels.

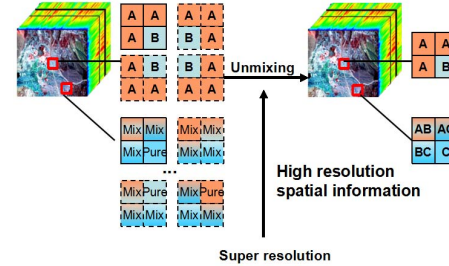


Fig. 2. Spatial resolution enhancement provides spatial information for endmember allocations.

II. JOINT SPATIAL RESOLUTION ENHANCEMENT AND SPECTRAL UNMIXING

In conventional approaches, spatial resolution enhancement and spectral unmixing have been treated separately. Such processing scheme tends to suffer from spectral distortions and spatial inconsistency. Unmixing performance is effected by artifacts in superresolution, while inaccurate spectral information leads to spectral distortions and degradation of spatial enhancement performance. In fact, spatial enhancement and spectral unmixing are correlated with some degree. Spatial resolution enhancement result can benefit spectral unmixing by acquiring high-resolution abundance maps and spatial regularization for endmember location. While unmixing can be used as significant spectral regularization in superresolution to reduce spectral distortions. Spatial resolution enhancement is expected to enhance spectral unmixing from the following three aspects that spatial superresolution.

- 1) *Reduces the Error of Spectral Mixing:* Since mixed pixels are inevitably caused by low spatial resolution, spatial resolution enhancement helps reduce the amount of mixed pixels. Fig. 1 illustrates that the amount of mixed pixels is reduced with increased spatial resolution. Both pure pixels and mixed pixels exist in the observed HSI. After spatial superresolution with a factor of n , a pure pixel is enlarged to $n \times n$ pure pixels containing the same endmembers. Mixed pixel I is also enlarged, but to $n \times n$ “pure” pixels with different endmember allocations. By providing more details of the land cover, spatial superresolution may achieve more pure pixels, which guarantees more accurate input of the subsequent unmixing step.
- 2) *Provides Spatial Information for Endmember Location:* Fig. 2 shows that spectral unmixing finds the endmembers and abundance maps in subpixel level. Proper spatial constraints, such as spatial correlation of the land cover, can be employed to unmixing to determine subpixel spatial location of endmembers.

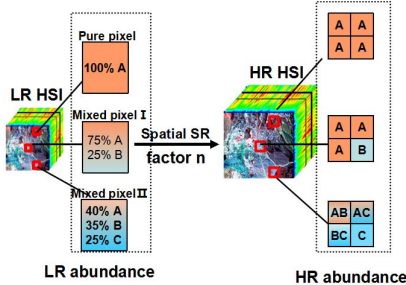


Fig. 3. Spatial resolution enhancement generates high-resolution abundance maps.

3) *Obtains High-Resolution Abundances*: Abundances represent the proportion of endmembers. Since the same endmembers are believed to locate in neighboring areas except for some edge regions in observed scenes, the noise and unmixing errors are presented as isolated points in the abundance maps. In Fig. 3, if the input to spectral unmixing has high spatial resolution and less spectral distortions, the abundance maps will have high spatial resolution and spatial consistency, which means that there should be less isolated points in the abundance maps. This improves the performance of sequential processing of object detection and classification.

Spectral unmixing improves the performance of spatial enhancement, since spectral unmixing:

1) *Reduces Spectral Distortions*: Although most spatial enhancement methods achieve good reconstruction results, the errors and artifacts from superresolution enhancement result in spectral distortions. And imperfection of hyperspectral sensors may cause spectral distortions in the original image. Spectral unmixing provides endmembers and abundances that are used as spectral regularization to reduce spectral distortions in superresolution enhancement [20].

2) *Estimates a Degradation Model*: The spatial resolution of abundance map is supposed to be consistent with the spatial resolution of the HSI. So the mapping scheme between high and low spatial resolution abundances can be utilized to create a model that describes the degradation between high spatial resolution HSI and its low-resolution version

$$A = WHB. \quad (1)$$

Here A and B denote the abundance maps of low- and high-resolution HSIs, respectively. WH represents the degradation factors from high- to low-resolution HSIs.

III. INTERACTIVE FEEDBACK OF SPATIAL SUPERRESOLUTION AND SPECTRAL UNMIXING

Spatial superresolution and spectral unmixing can be employed to regularize each other for enhanced resolutions in the spatial and spectral domain. This paper presents an HSI spatial resolution enhancement algorithm, denoted as JHSr-Un, based on interactive feedback of spatial superresolution enhancement and spectral unmixing with the following two conditions.

- 1) The endmembers should not change before and after spatial resolution enhancement.
- 2) The mapping scheme (down-sampling and blurring) of abundance maps before and after superresolution should be the same as the degradation mapping of low and high HSIs.

Fig. 4 shows that the interactive feedback framework can be used to simultaneously improve superresolution and unmixing performances. Initially given a high-resolution HSI, the endmembers and high-resolution abundances are acquired from spectral unmixing. The unmixing result can also generate high-resolution HSI. If the unmixing is accurate, the endmembers and abundances are supposed to generate a high-resolution HSI that is close to the input. Therefore, the spatial difference between the high-resolution HSI achieved by superresolution and the high-resolution HSI generated by unmixing result is utilized to control spectral unmixing. From a different perspective, spectral priors provided by unmixing are used to regularize spatial enhancement. Endmembers are assumed to be the same before and after spatial enhancement, while the high- and low-abundances obey the spatial degradation relationship. Therefore, the spectral deviation before and after spatial enhancement is used as feedback in superresolution to reduce spectral distortions. As the reconstruction quality goes up, the spatial differences and spectral deviations decrease to guarantee the stability of both spatial superresolution and spectral unmixing. Therefore, the interactive feedback framework can iteratively solve superresolution and unmixing, achieving more accurate resolution enhancement and better unmixing results of an HSI.

A. Degradation Model and Sparse Superresolution

Low spatial resolution HSI with m pixels and L spectral bands is denoted as an $m \times L$ matrix $Y \in R^{m \times L}$ and high-resolution HSI with M pixels and L bands is denoted as an $M \times L$ matrix $X \in R^{M \times L}$. Both X and Y are represented in 2-D forms. Each column of Y and X represents each band of the low- and high-resolution image. The spatial degradation model is represented as follows:

$$Y = WHX + v \quad (2)$$

where $v \in R^{m \times L}$ denotes an additive Gaussian noise, $W \in R^{m \times M}$ is the spatially down-sampling operator, and $H \in R^{M \times M}$ is the spatially blurring operator caused by atmospheric turbulence or other factors [20].

According to sparse representation, spatial superresolution problem can be formulated as

$$\alpha = \arg \min \{ \|Y - WHD \circ \alpha\|_F^2 + \lambda \|\alpha\|_0\}. \quad (3)$$

D is the high-resolution dictionary trained using a series of panchromatic images via the K-means singular value decomposition (K-SVD) algorithm [29]. If the size of high-resolution image patch is assumed to be $c \times c$, the size of D is $c^2 \times d$, where d denotes the number of dictionary atoms. And α_i is the sparse coefficient vector over the dictionary D .

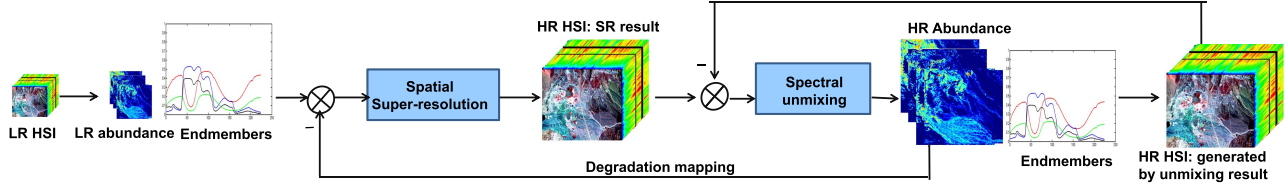


Fig. 4. Interactive feedback scheme of hyperspectral superresolution and unmixing.



Fig. 5. Sample panchromatic images used for dictionary learning.

By substituting (2) and (3), the operator \circ is defined as [30]

$$D \circ \alpha = \left(\sum_{i=1}^P R_i^T R_i \right)^{-1} \sum_{i=1}^P (R_i^T D \alpha_i) \quad (4)$$

where R_i is the patch extracting matrix, i denotes the number of patches, $i = 1, 2, \dots, P$. Assume that $x_i = D \alpha_i$ represents the high-resolution image patch, α_i is the sparse coefficient vector. The high-resolution X can be reconstructed by averaging all of the reconstructed high-resolution patches. So α is the concatenation of all α_i [30]. The sparse coefficient parameter is a positive parameter which is used to balance the tradeoff between reconstruction accuracy and the sparseness. This parameter is generally dependent on the noise level. And the Frobenius norm $\|\bullet\|_F^2$ enforces the data fidelity while the l_0 norm $\|\bullet\|_0$ acts as sparse constraint. However, the l_0 norm is not convex and it cannot achieve a unique solution, so (3) is an NP-hard problem. In order to ensure the uniqueness of the solution, l_0 norm should be relaxed to l_1 norm when the coefficient α is sufficiently sparse [31]

$$\alpha = \arg \min \{ \|Y - WHD \circ \alpha\|_F^2 + \lambda \|\alpha\|_1\}. \quad (5)$$

The fusion of panchromatic images and HSI has been an efficient way to enhance spatial resolution [32]. The abundant high spatial resolution patterns contained in panchromatic image can provide spatial structures to ensure the accuracy of the enhanced HSI. Known from sparse representation, an over-completed dictionary is believed to preserve overall spatial features in its atoms and is used to reconstruct high spatial resolution images. While it is always difficult to acquire panchromatic image with the same scene of HSI, panchromatic images of other scenes are utilized for spatial dictionary learning. In order to learn a comprehensive and representative dictionary, the training images should contain enough spatial characteristics which are similar to the observed scene. If the observed HSI captures a natural scene, the training images should be a series of different panchromatic images which also capture the natural scenes. Although the actual objects in the panchromatic images are quite different than those in the observed HSI, it has been found that the microstructures of images can be represented by a small numbers of structural primitives, such as object edges, line segments, and other elementary features, and these primitives are qualitatively similar

in similar type of scenes [20]. In this paper, dictionary learning has been done using the extracts of Quickbird panchromatic images which are not related to and do not overlap with the HSI to be enhanced. Fig. 5 shows some of the Quickbird panchromatic images used for dictionary learning.

B. Sparse Spectral Unmixing

Spectral mixing is inevitable in HSI due to the low spatial resolution. According to the spectral mixing model, mixed pixel is decomposed into a linear combination of endmembers which are weighted by a set of fraction abundances [33]. As for the desired high-resolution HSI $X \in R^{M \times L}$, the spectral mixing model can be described in a linear regression form

$$X = BS + \omega \quad (6)$$

where each column of X represents measured spectrum of one pixel. $S \in R^{K \times L}$ contains K pure endmembers, $B \in R^{M \times K}$ represents fraction abundances, and $\omega \in R^{M \times L}$ denotes the noise or model error. Spectral unmixing can be solved with sparse regression using material spectra achieved in the United States Geological Survey (USGS) library [34]. A sparse mixture model is given by [34]

$$B = \arg \min \|X - BS\|_F^2 + \varepsilon \|B\|_1 \quad (7)$$

where S is the given spectral library. The abundance B is regularized using sparsity constraint. Most elements in S are zeros or close to zero due to the sparsity prior. The abundance is added with abundance nonnegativity constraint. While the other linear unmixing regularization abundance sum-to-one constraint (ASC) is not satisfied in sparse unmixing. If ASC is imposed on the abundance matrix B , the unmixing problem will not depend on the sparse regression term $\|B\|_1$ because the sum of elements in each column of B is always equal to 1 [34]. And the parameter ε is the weight of sparsity of unmixing which is dependent with the noise level.

C. Joint Spatial Superresolution and Unmixing

Spatial superresolution recovers high spatial resolution of HSI from its low resolution version Y . Superresolution and unmixing are alternately carried out with interactive feedback to obtain high spatial resolution and spectral unmixing results (spatial sparse coefficient α and abundance map B).

Spectral signatures obtained from unmixing are assumed to be exactly the same as the spectral signatures after sparse superresolution. So here is a constraint that the spatial expression $D \circ \alpha$ of original HSI should be approximate to the spectral expression BS

$$\min \|D \circ \alpha - BS\|_F. \quad (8)$$

Linear unmixing is employed to regularize the solution space to preserve spectral consistency and suppress noise [20]. The spectral regularization is combined with a least squares optimization term

$$\{\hat{\alpha}, D, B, S\} = \arg \min \|Y - \text{WHD} \circ \alpha\|_F^2 + \lambda_1 \|X - BS\|_F^2 + \lambda_2 \|\alpha\|_1. \quad (9)$$

By substituting (6) into (9)

$$\{\hat{\alpha}, D, B, S\} = \arg \min \|Y - \text{WHD} \circ \alpha\|_F^2 + \lambda_1 \|D \circ \alpha - BS\|_F^2 + \lambda_2 \|\alpha\|_1 \quad (10)$$

where λ_1 is used to weight the difference between spectral signatures from superresolution and unmixing.

Therefore, the objective function is formulated as

$$\{\hat{\alpha}, B\} = \arg \min \|Y - \text{WHD} \circ \alpha\|_F^2 + \lambda_1 \|D \circ \alpha - BS\|_F^2 + \lambda_2 \|\alpha\|_1 + \lambda_3 \|B\|_1 \quad (11)$$

where the second term denotes a fidelity term. λ_2 is used to weight the difference between spectral signatures from superresolution and unmixing. λ_3 represents the sparsity of abundance.

D. Solutions to Objective Function

The solution to (11) is unique when the objective is convex. As (11) is convex when the corresponding dictionary or spectral library is fixed, the objective function is ascertained to have unique solution. To solve (11), variable splitting and alternate optimization are utilized to deal with multiple variables objective function [35]. The optimization problem can be divided into the following two subproblems regularized with l_1 norm. To solve sparse coefficient α by fixing B

$$\hat{\alpha}_{(i)} = \arg \min \|Y - \text{WHD} \circ \alpha\|_F^2 + \lambda_1 \|D \circ \alpha - B_{(i-1)} S\|_F^2 + \lambda_2 \|\alpha\|_1. \quad (12)$$

The spatial sparse coefficient at i th iteration is solved with the addition of spectral constraint. By letting $\tilde{Y} = \begin{bmatrix} Y \\ \lambda_1 B_{(i-1)} S \end{bmatrix}$ and $\psi = \begin{bmatrix} \text{WHD} \\ \lambda_1 D \end{bmatrix}$, (12) can be rewritten as

$$\hat{\alpha}_{(i)} = \arg \min \|\tilde{Y} - \psi D \circ \alpha\|_F^2 + \|\alpha\|_1. \quad (13)$$

This optimization function of $\alpha_{(i)}$ is based on sparse coding. Generally, the optimization problem can be solved by alternately learning D using K-SVD method [28] and inferring α_i using the orthogonal matching pursuit [36]. To solve abundance B by fixing α , the abundance map is estimated with respect to the given spectral library based on sparse unmixing

$$B_{(i)} = \arg \min \lambda_1 \|D \circ \alpha - BS\|_F^2 + \lambda_3 \|B\|_1 \quad i = 1, 2, 3, \dots \quad (14)$$

By transposing B to find a unique solution using iterative shrinkage-shareholding method [37] or the split augmented Lagrangian shrinkage algorithm method [35]

$$B_{(i)} = \arg \min \{\|(D \circ \alpha)^T - S^T B^T\|_F^2 + \lambda_3 / \lambda_1 \|B\|_1\} \text{ s.t. } B > 0 \quad i = 1, 2, 3, \dots \quad (15)$$

Algorithm 1 Joint Hyperspectral Super-Resolution and Unmixing with Interactive Feedback (JHSr-Un)

Input: Low resolution HSI Y , dictionary D , USGS library S

Initialization: Set $i = 1$, solve initial $\hat{\alpha}_0$ using

$$\hat{\alpha}_0 = \arg \min \|Y - \text{WHD} \circ \alpha\|_F^2 + \lambda \|\alpha\|_1$$

obtain the initial high resolution HSI $X_0 = D\hat{\alpha}_0$

Begin:

While $i \leq \text{max iteration count}$

1) Obtain the sparse coefficient α_i using (13) with respect to B_{i-1} : $\alpha_{(i)} = \arg \min \{\|\tilde{Y} - \psi D \circ \alpha\|_F^2 + \|\alpha\|_1\}$ where $\tilde{Y} = \begin{bmatrix} Y \\ \lambda_1 B_{(i-1)} S \end{bmatrix}$, $\psi = \begin{bmatrix} \text{WHD} \\ \lambda_1 D \end{bmatrix}$.

2) Obtain the abundance $B_{(i)}$ using (15) with respect to α_i :

$$B_{(i)} = \arg \min \{\|(D \circ \alpha)^T - S^T B^T\|_F^2 + \lambda_3 / \lambda_1 \|B\|_1\} \text{ s.t. } B > 0 \quad i = 1, 2, 3, \dots$$

3) Update the high resolution HSIs $X_{(i)}$: $X_{(i)} = D\alpha_{(i)}$.

4) $i = i + 1$

End

Output: High spatial resolution HSI $X_{(i)}$, Abundance $B_{(i)}$ of $X_{(i)}$.

The above subproblems are processed repeatedly until the stopping criterion is met. The iteration stopping condition can be set as the maximum number of iterations, longest iteration time or maximum iteration error. Here variable splitting and alternate optimization are utilized to deal with multiple variables problems [35], (13) and (15) will be alternately solved until the iteration stopping condition is met. The iteration stops when the maximum iteration count is reached. The proposed superresolution and unmixing with interactive feedback algorithm method is outlined as Algorithm 1.

IV. EXPERIMENTS AND RESULTS

A. Methods and Performance Evaluation Measures for Comparison

To confirm the proposed method, we compare our JHSr-Un method with state-of-the-art techniques in terms of superresolution and spectral unmixing on both simulated and real data sets. The superresolution methods used for comparison are POCS [15], Distance-based Similarity Measure for Variational Model (DSVM) [38], SparseFI [21], and Joint Nonlocal Similarity (SFTD) [20]. To apply POCS method which is designed for angular HSI processing [15], we down-sampled the original HSI and simulated multiangular images by shifting. As for DSVM, SparseFI and SFTD, only one image is used as input.

The unmixing methods for comparison are fully constrained least squares (FCLS) [39], sparse unmixing algorithm via variable splitting and augmented Lagrangian (SUnSAL) [34],

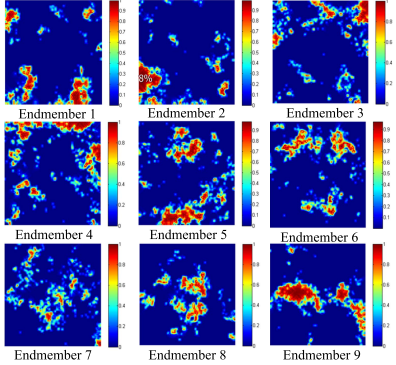


Fig. 6. Examples of nine abundance of simulated HSI data set.

and sparse unmixing algorithm via variable SUnSAL-total variation (SUnSAL-TV) [40]. All these methods used the same inputs as our proposed method, and the spectral library used in SUnSAL, SUnSAL-TV and the proposed method are also the same. The performance of the spatial superresolution is measured using peak signal-to-noise ratio (PSNR), structural similarity index (SSIM), and feature similarity index (FSIM) that assess reconstruction quality, structure information carrying in dependent pixels and local features, respectively [20]. The quality of the reconstruction of spectral mixing are measured using the signal-to-reconstruction error (SRE) [34]

$$SRE(\text{in dB}) = 10 \log_{10}(\|X\|_2^2 / \|X - \hat{X}\|_2^2) \quad (16)$$

where X and \hat{X} represent the ground-truth and estimated value of abundances in HSI, respectively. spectral angle mapper (SAM) index is used to measure spectral distortion. Smaller values of SAM and higher values of PSNR, SSIM, FSIM, and SRE show improved performances. In the proposed method, the training panchromatic images are sampled into 15 000 raw high spatial resolution patches of size 8×8 , which are then trained using K-SVD method. The number of dictionary atoms is 256.

B. Experiments on Simulated Data Set

HSIs of a simulated data set are generated using a spectral linear mixed model, randomly selecting signatures as endmembers from the USGS spectral library with the abundance sum-to-one constraint. Simulated HSIs of size $100 \times 100 \times 224$ contains nine endmembers, their corresponding ground-truth abundances are shown in Fig. 6. The abundances are smooth with sharp transitions, which exhibit spatial homogeneity and show the true abundances of endmembers [34]. Their low-resolution degraded versions are generated by applying a truncated 7×7 Gaussian kernel with the standard deviation of 0.5 followed by a downsampling factor of 3.

As indicated from the objective function in (11), the unmixing result can provide spectral constraint to reduce spectral distortions in superresolution. Although both sparse spatial result $D\alpha$ and unmixing result BS can be considered as spatial enhancement result, only the result of sparse coding in (13) is used as the final superresolution result. The high-resolution image generated by unmixing result is also compared with

TABLE I
EVALUATION OF SPATIAL ENHANCED RESULTS
ON SIMULATED HSI DATA SET

	POCS	DSVM	Sparse -FI	SFTD	JHSr-Un	SUnSAL
MSPNR	33.472	34.057	38.360	41.062	41.452	40.998
MSSIM	0.741	0.762	0.848	0.874	0.923	0.830
MFSIM	0.784	0.812	0.891	0.911	0.944	0.895
MSA	0.050	0.039	0.045	0.032	0.023	0.026

TABLE II
EVALUATION OF SPECTRAL UNMIXING RESULTS
ON SIMULATED HSI DATA SET

	FCLS	SUnSAL	SUnSAL-TV	JHSr-Un
SRE	10.8030	10.8326	10.9952	11.2206

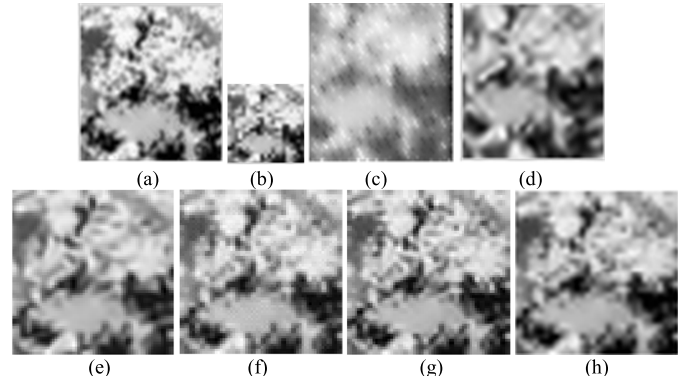


Fig. 7. Spatially enhanced images of band 50 on the simulated data set. (a) Original HR image. (b) Original simulated LR image. Superresolution enhancement results by (c) POCS, (d) DSVM, (e) SparseFI, (f) SFTD, (g) JHSr-Un, and (h) SUnSAL.

JHSr-Un method. In order to make a fair comparison with the proposed method, the sparse unmixing method SUnSAL with l_1 -norm regression on abundance is used, same as in the unmixing step in the proposed method. The evaluation measurements of spatial enhancement and unmixing are presented in Tables I and II, which show that our proposed JHSr-Un method can simultaneously achieve better spatial enhancement results and unmixing results than other compared methods due to the proposed feedback framework. Average performance indices PSNR, SSIM, FSIM, and SAM in Table I are used to evaluate spatial enhancement performance. SRE listed in Table II is used to assess spectral unmixing results. The best results for each index are written in bold letters.

POCS is a typical spatial domain superresolution method. It produces inferior results of the mean values of PSNR, SSIM, and FSIM (Table I). POCS uses convex sets as prior spatial constraints to obtain high-resolution result. Since the intersection of all the convex sets is not always unique, high-resolution images are not unique as well. And POCS requires high accuracy in motion estimation. Inaccurate motion estimation will result in slow and instable convergence. The

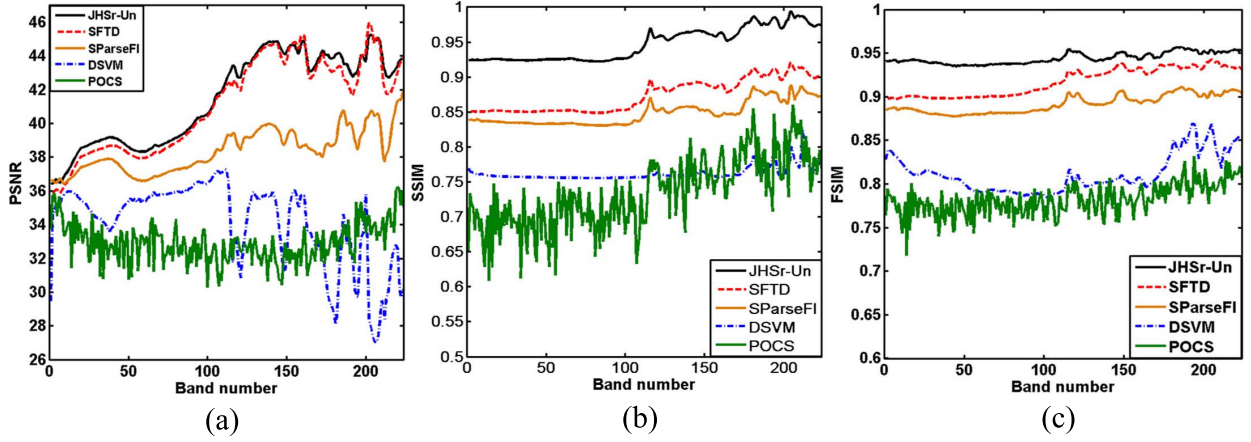


Fig. 8. Spatial assessment curves of simulated data set. (a) PSNR. (b) SSIM. (c) FSIM.

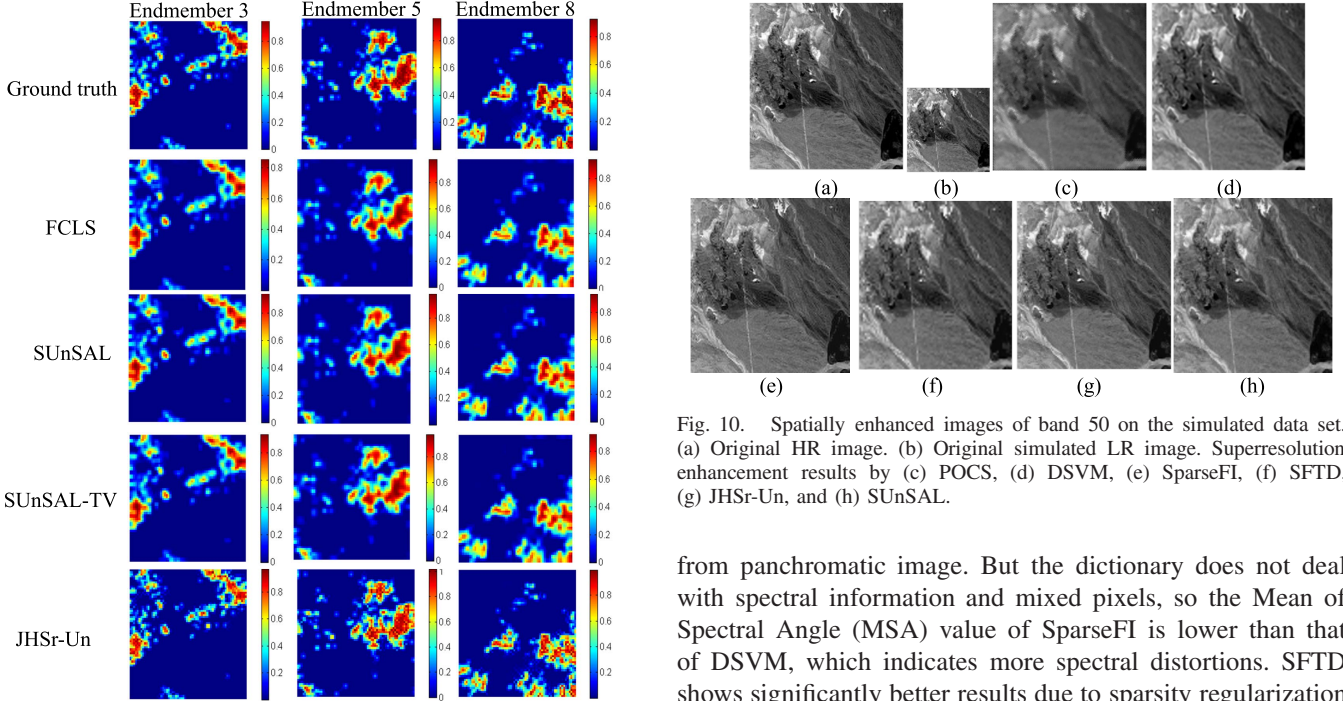


Fig. 9. Unmixing results of endmembers 3, 5, and 8 of simulated data set HSI3. Original abundance maps were used as ground truth. From top to bottom: ground truth, FCLS, SUnSAL, SUnSAL-TV, and JHSr-Un.

mean value of SAM in Table I shows that POCS has serious spectral distortions because there are no powerful spectral constraints. Although DSVM has comparable results in spatial evaluation indices as POCS, DSVM outperforms POCS in spectral fidelity. DSVM is designed with a spectral preservation function and a gray value constraint to ensure that the fused image is close to the original HSI and panchromatic image. However, since DSVM does not consider mixed pixels in HSI, to the result is missing spectral information. The DSVM chooses one band from the HSI as the panchromatic image for dictionary learning when real panchromatic image is unavailable, which also degrades the superresolution performance. SparseFI shows superior spatial enhancement than DSVM due to the high-resolution dictionary trained

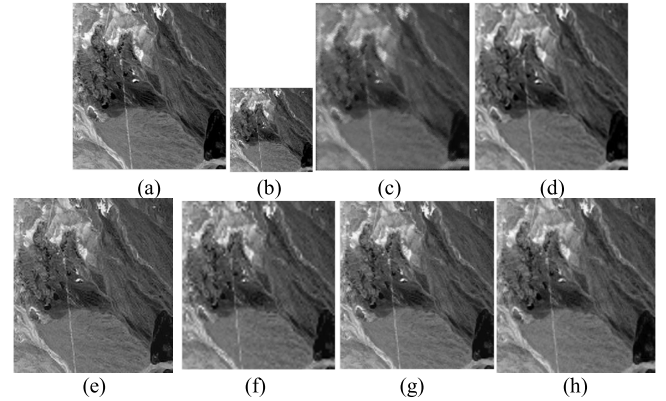


Fig. 10. Spatially enhanced images of band 50 on the simulated data set. (a) Original HR image. (b) Original simulated LR image. Superresolution enhancement results by (c) POCS, (d) DSVM, (e) SparseFI, (f) SFTD, (g) JHSr-Un, and (h) SUnSAL.

from panchromatic image. But the dictionary does not deal with spectral information and mixed pixels, so the Mean of Spectral Angle (MSA) value of SparseFI is lower than that of DSVM, which indicates more spectral distortions. SFTD shows significantly better results due to sparsity regularization and nonlocal information on spatial and spectral structures. The assessment indices of high-resolution image generated by SUnSAL unmixing results is also presented in Table I. SUnSAL is a sparse regression unmixing method which deals with mixed pixels and preserves spectral information. JHSr-Un benefits from the feedback term $\|D \circ \alpha - BS\|_F^2$, where spectral signatures obtained from unmixing are the same as the spectral signatures after superresolution. As superresolution and unmixing are alternately processed with the proposed JHSr-Un method, spectral constraints guarantee spectral consistency with reduced spectral distortions. In Fig. 7, spatial resolution enhancement results of selected band are shown. The enhanced image of POCS [Fig. 7(c)] is seriously blurred. JHSr-Un method [Fig. 7(g)] achieves better visual quality than the other methods with sharper edges and clearer textures. The superiority of JHSr-Un can also be seen in Fig. 8 where spatial evaluation indices values of each band are presented in terms of PSNR, SSIM, and FSIM.

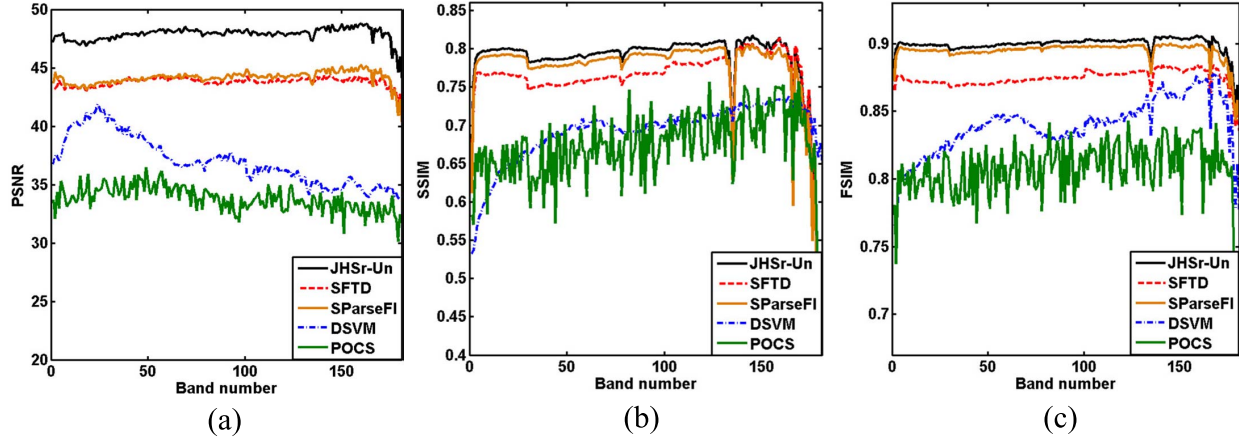


Fig. 11. Spatial assessment curves of real data set. (a) PSNR. (b) SSIM. (c) FSIM.

The proposed method demonstrates successful spectral unmixing results. The highest values of SRE written in bold in Table II indicate that the least spectral distortion and reconstruction spectral error were achieved. Visually, the abundances of the proposed method are closest to the ground truth. In addition, clearer contours, sharper abundance maps, and less isolated points are also found with the proposed method in Fig. 9. The interactive feedback scheme uses spatially enhanced results as the input to spectral unmixing. FCLS is a least squares algorithm which imposes only nonnegativity constraint and sum-to-one constraint without any other regulations, therefore SRE is low and the abundance maps are visually inaccurate. When the sparsity of abundance on a given spectral library is employed in the semisupervised SUNSAL method on a linear spectral mixture model, a better unmixing result was obtained compared to FCLS. While the analysis based on sparse regression without incorporating spatial information does not guarantee consistency in spatial domain, the total variation constraint has preserved spatial correlation in SUNSAL-TV method that results in better unmixing result compared to SUNSAL.

C. Experiments on Real Data Set

A real data set consists of HSI of cuprite in 224 spectral bands in the 400–2500 nm range, captured by the Airborne Visible/Infrared Imaging Spectrometer sensor over cuprite mine district in Nevada. We extract subimages of size 256×256 to reduce computational burden. Images of bands 1–3, 104–116, 148–170, and 221–224 are left out due to heavy noise and low quality, so the size of the final HSI set is $256 \times 256 \times 181$. Quantitative measures for spatial superresolution are shown in Table III where the best ones are written in bold. Average performance indices Mean of Peak Signal to Noise Ratio (MPSNR), Mean of Structural Similarity Index (MSSIM), Mean of Feature Similarity Index (MFSIM) are used to evaluate spatial enhancement performance. And MSA is used to evaluate spectral distortions. Like the simulated experiments, the high-resolution image generated by SUNSAL is also compared with the proposed method. POCS shows relatively poor reconstruction quality with serious spectral distortions. DSVM achieves better performance

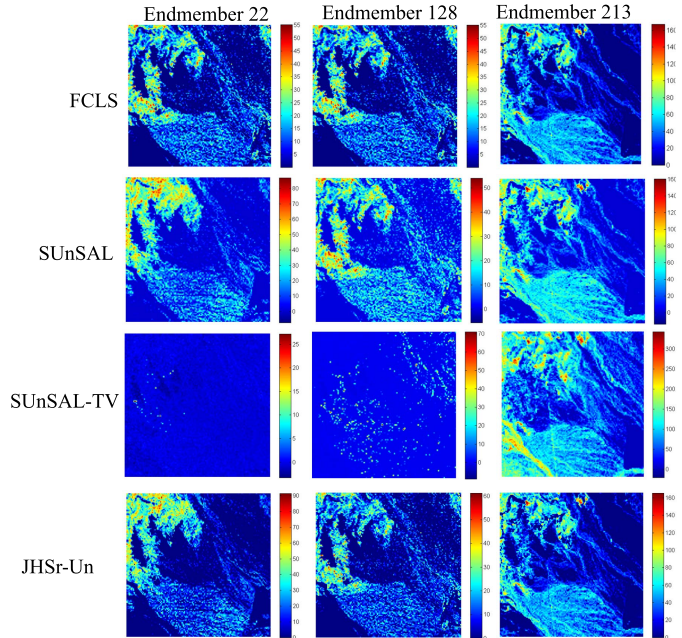


Fig. 12. Unmixing results of endmember 22, 128, and 213 of the real data set. The original abundance maps are used as ground truth. From top to bottom: ground truth, FCLS, SUNSAL, SUNSAL-TV, and JHSr-Un.

than POCS due to its geometric function and spectral preservation. It is worth to note that the panchromatic image used in SparseFI is simulated by linearly combining the original high spatial resolution hyperspectral band images. While the dictionary in our proposed JHSr-Un is trained by Quickbird panchromatic images acquired from different scenes. Further experiments have been done to understand the influence of different training data sets. The indices in Table IV show the comparison of SparseFI and JHSr-Un with varying dictionary training data sets (Quickbird panchromatic images, simulated panchromatic image, and Quickbird and simulated panchromatic images). Both SparseFI and JHSr-Un have higher index values when simulated panchromatic image is used for dictionary learning, which indicates that better performance can be achieved if training data set covers the same location as the input hyperspectral data set. JHSr-Un proves superior to SparseFI and SFTD

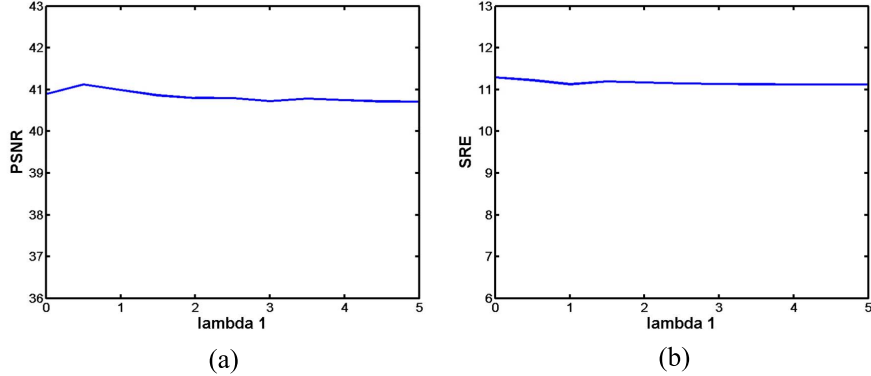


Fig. 13. Sensitivity analysis on simulated data set of (a) superresolution performance and (b) unmixing performance when λ_1 varies.

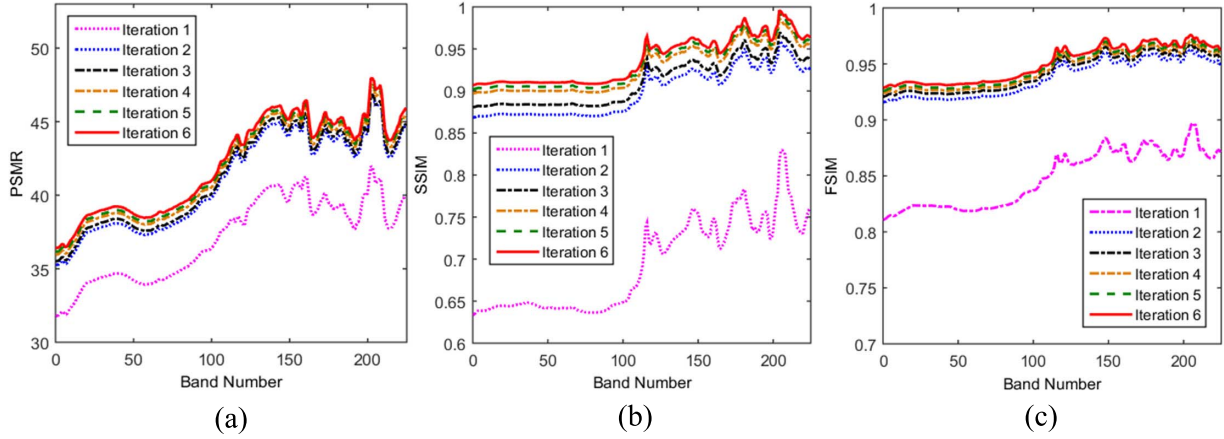


Fig. 14. Assessments curves of simulated data set in each iteration. (a) PSNR. (b) SSIM. (c) FSIM.

TABLE III

EVALUATION OF SPATIAL ENHANCED RESULTS ON REAL DATA SET

	POCS	DSVM	Sparse -FI	SFTD	JHSr- Un	SUnSAL
MSPNR	36.259	37.017	44.266	43.802	47.911	37.107
MSSIM	0.684	0.692	0.772	0.769	0.783	0.751
MFSIM	0.831	0.839	0.893	0.878	0.905	0.879
MSA	0.145	0.118	0.110	0.102	0.094	0.118

according to Tables III and IV, which demonstrates the effectiveness of proposed feedback framework.

Fig. 10 shows the superresolution results of selected band. The proposed JHSr-Un method shows better spatial enhancement performance by visual inspection and in terms of average evaluation values. The JHSr-Un method demonstrated clearer details than other algorithms. Fig. 11 shows the spatial evaluation indices values in each band. The evaluation values of JHSr-Un in most bands are higher than other state-of-the-art superresolution methods. Fig. 12 shows the unmixing results on the abundance maps of endmembers 22, 128, and 213. The proposed JHSr-Un method has generated sharper and higher resolution abundance maps with less isolated points than other methods, indicating that the spectral unmixing results can be improved with enhanced spatial resolution.

TABLE IV

EVALUATION OF SparseFI AND JHSr-UN WITH DIFFERENT TRAINING DATA SETS

Training dataset	Index	Sparse-FI	SFTD
Quickbird image	MPSNR	44.266	47.911
	MSSIM	0.772	0.783
	MFSIM	0.893	0.905
Simulated PAN	MPSNR	44.618	47.920
	MSSIM	0.811	0.804
	MFSIM	0.903	0.906
Quickbird& Simulated PAN	MPSNR	44.194	47.913
	MSSIM	0.773	0.789
	MFSIM	0.893	0.905

D. Parameter Setting and Sensitivity Analysis

1) *Parameter Setting of the Proposed Method:* As shown in (11), the objective function of our proposed JHSr-Un method has three parameters. The first parameter λ_1 is the weight of disparity of spatial and spectral, which determines the weight of BS in (12) when we solve the sparse coefficient α in each iteration. We present the sensitivity analysis for this parameter. As shown in Fig. 13, the mean PSNR and SRE indexes are given by varying λ_1 from 0.1 to 5, which indicates that the changes of these indexes are insignificant. It

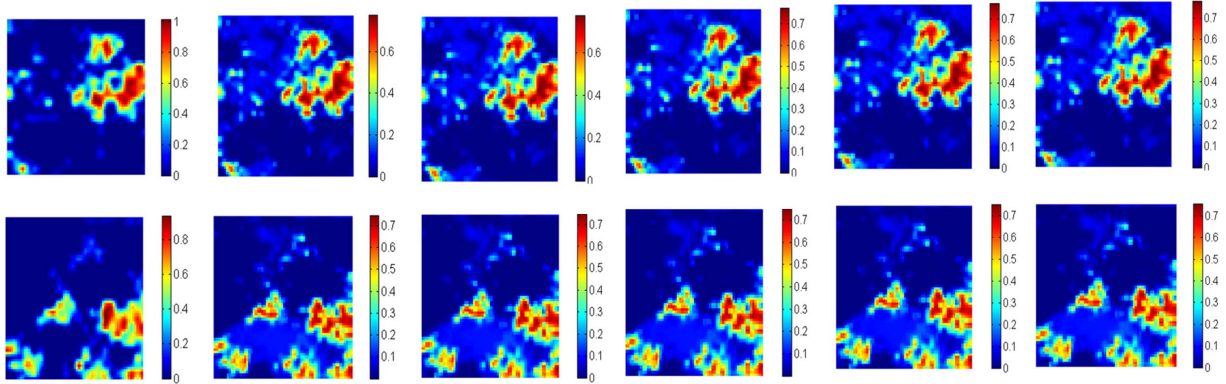


Fig. 15. Abundances of endmembers 5 and 8 of the simulated data set. From left to right: abundances from iteration 1 to iteration 6. From top to bottom: endmember 5 and endmember 8.

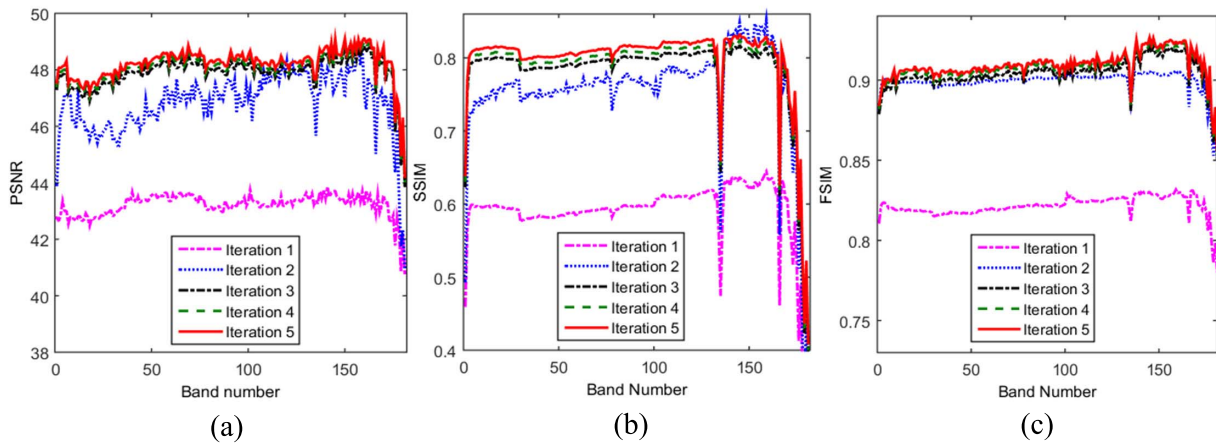


Fig. 16. Assessments curves of real data set in each iteration. (a) PSNR. (b) SSIM. (c) FSIM.

is clear that the proposed method is insensitive to parameter λ_1 . The spatial superresolution and the unmixing performance are proved to be robust with parameter λ_1 set in the range of $[0.1, 5]$. So λ_1 is finally set at the fixed value 0.5 in our experiments. The second parameter is the sparse coefficient parameter λ_2 , which balances the sparsity and representation error in (11). It is usually set to a small value (0.001–0.0001) for superresolution reconstruction [22], [23]. In this experiment we fix this parameter at 0.0025. The third parameter is λ_3 , it is the weight of sparsity for unmixing. The ratio λ_3/λ_1 in (15) depends on the noise level in HSI, if the noise level is high, this ratio should be set to a relative large value, and vice versa. According to the parameter setting in [34], we fix λ_3/λ_1 as 0.00075 in our experiment.

2) *Parameter Setting of Compared Methods*: The parameter setting of the compared algorithms first follow suggestions from the authors, and then they are empirically tuned to achieve the best result. For the compared superresolution methods, we adopted all default values for parameter setting of the POCS algorithm. The performance of DSVM method is sensitive to the parameter of distance-based similarity measure which is set as 0.05 in our experiment, while the other parameter values are adopted according to the authors' suggestions. As for the SparseFI method, we set the parameter of sparse coefficient as 0.002 and follow the authors' suggestions on

the rest of parameters. The SFTD method achieves the best result when the sparse parameter and nonlocal parameter are set as 0.005 and 0.01, respectively. For the compared unmixing methods, there is no parameter to tune for the FCLS method. For the SUnSAL method, the parameter to be tuned is the weight of abundance sparsity, which depends on the noise level. This parameter is set as 0.00075, the same as λ_3/λ_1 for our proposed method. For the SUnSAL-TV method, the weight of sparsity and the weight of TV constraint are dependent on the noise level, we set these parameters as 0.00075 and 0.0001, respectively.

E. Efficiency Validation

To validate the efficiency of the proposed JHSr-Un method, spatial and spectral results for the simulated data set are presented at each iteration in Table V. We observed that spatial and spectral performance increased dramatically usually after the first and second iterations, then reached a plateau. Fig. 14 shows the evaluation values at each band for six iterations. Fig. 15 shows unmixing results for two endmembers. Progressive unmixing results for six iterations show how spectral performances have been improved after each iteration using the interactive feedback scheme.

TABLE V
AVERAGE SPATIAL AND SPECTRAL EVALUATION
MEASUREMENTS FOR A SIMULATED DATA SET

	Iter. 1	Iter. 2	Iter. 3	Iter. 4	Iter. 5	Iter. 6
PSNR	37.08	41.01	41.28	41.30	41.39	41.45
SSIM	0.69	0.89	0.91	0.92	0.92	0.92
FSIM	0.84	0.93	0.94	0.94	0.94	0.94
SAM	0.03	0.02	0.02	0.02	0.02	0.02
SRE	10.50	11.04	11.12	11.17	11.21	11.23

TABLE VI
AVERAGE SPATIAL AND SPECTRAL EVALUATION
MEASUREMENTS FOR A REAL DATA SET

	Iter. 1	Iter. 2	Iter. 3	Iter. 4	Iter. 5
PSNR	43.21	46.84	47.90	47.91	47.91
SSIM	0.59	0.75	0.78	0.78	0.78
FSIM	0.82	0.89	0.90	0.90	0.90
SAM	0.12	0.10	0.09	0.09	0.09

The superresolution results for each iteration of the real data set are shown in Table VI and the assessment curves are shown in Fig. 16. Spatial and spectral performance increased dramatically in the first and second iterations, then they stopped improving. If the iteration number is too large, the results may deteriorate. It is the same as what we observed from the simulated data set, the reasons are over-fitting in sparse coding and over-smoothing during unmixing stages. The improved results again show the benefit of the feedback framework.

V. CONCLUSION

This paper presents JHSr-Un with interactive feedback. Spatial and spectral regularizations are applied to each other as priors to alternately generate spatial and spectral results for mutual enhancement. In this algorithm, unmixing results reduce spectral distortions and guarantee spectral correlation while the enhanced results of spatial superresolution are used as higher resolution input of unmixing to improve spectral performance. Experiments on both simulated and real data sets have demonstrated that the proposed JHSr-Un method achieves higher spatial and spectral results than stand-alone state-of-the-art methods. The advantages of interactive feedback framework are summarized as:

- 1) *Interactive Feedback Improves the Performance of Both Spatial Superresolution and Spectral Unmixing:* Superresolution enhancement finds a high-resolution HSI, which will be used as an input to subsequent spectral unmixing to increase spectral resolution. Enhanced spectral unmixing results will then be used in the next superresolution step.
- 2) *Interactive Feedback Reduces Errors and Artifacts:* Spatial and spectral deviations are employed as a prior to control spatial resolution enhancement and spectral unmixing

- 3) *Interactive Feedback:* It is applicable to other superresolution algorithms where spectral unmixing is applied.

REFERENCES

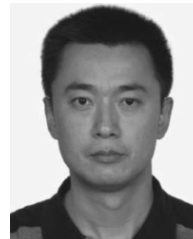
- [1] Y. Zhao, C. Yi, J. Yang, and J. C.-W. Chan, "Coupled hyperspectral super-resolution and unmixing," in *Proc. IEEE Geosci. Remote Sens. Symp. (IGARSS)*, Jul. 2014, pp. 2641–2644.
- [2] J. Yang, Y.-Q. Zhao, J. C.-W. Chan, and S. G. Kong, "Coupled sparse denoising and unmixing with low-rank constraint for hyperspectral image," *IEEE Trans. Geosci. Remote Sens.*, vol. 54, no. 3, pp. 1818–1833, Mar. 2016.
- [3] H. Zhang, W. He, L. Zhang, H. Shen, and Q. Yuan, "Hyperspectral image restoration using low-rank matrix recovery," *IEEE Trans. Geosci. Remote Sens.*, vol. 52, no. 8, pp. 4729–4743, Aug. 2014.
- [4] Y.-Q. Zhao and J. Yang, "Hyperspectral image denoising via sparse representation and low-rank constraint," *IEEE Trans. Geosci. Remote Sens.*, vol. 53, no. 1, pp. 296–308, Jan. 2015.
- [5] A. S. Charles, B. A. Olshausen, and C. J. Rozell, "Learning sparse codes for hyperspectral imagery," *IEEE J. Sel. Topics Signal Process.*, vol. 5, no. 5, pp. 963–978, Sep. 2011.
- [6] D. Lorente, N. Aleixos, J. Gómez-Sanchis, S. Cubero, O. L. García-Navarrete, and J. Blasco, "Recent advances and applications of hyperspectral imaging for fruit and vegetable quality assessment," *Food Bioprocess Technol.*, vol. 5, no. 4, pp. 1121–1142, May 2012.
- [7] P. W. Yuen and M. Richardson, "An introduction to hyperspectral imaging and its application for security, surveillance and target acquisition," *Imag. Sci. J.*, vol. 58, no. 5, pp. 241–253, 2010.
- [8] F. D. van der Meer *et al.*, "Multi- and hyperspectral geologic remote sensing: A review," *Int. J. Appl. Earth Observ. Geoinf.*, vol. 14, no. 1, pp. 112–128, Feb. 2012.
- [9] A. Plaza *et al.*, "Recent advances in techniques for hyperspectral image processing," *Remote Sens. Environ.*, vol. 113, no. 1, pp. S110–S122, 2009.
- [10] Q. Yuan, L. Zhang, and H. Shen, "Hyperspectral image denoising employing a spectral-spatial adaptive total variation model," *IEEE Trans. Geosci. Remote Sens.*, vol. 50, no. 10, pp. 3660–3677, Oct. 2012.
- [11] R. M. Willett, M. F. Duarte, D. A. Davenport, and R. G. Baraniuk, "Sparsity and structure in hyperspectral imaging: Sensing, reconstruction, and target detection," *IEEE Signal Process. Mag.*, vol. 31, no. 1, pp. 116–126, Jan. 2014.
- [12] K. Atkinson, F. Kamalabadi, and L. J. Douglas, "Wavelet-based hyperspectral image estimation," in *Proc. IEEE Geosci. Remote Sens. Symp. (IGARSS)*, vol. 2, Jul. 2003, pp. 743–745.
- [13] R. H. Chan, T. F. Chan, L. Shen, and Z. Shen, "Wavelet algorithms for high-resolution image reconstruction," *SIAM J. Sci. Comput.*, vol. 24, no. 4, pp. 1408–1432, 2003.
- [14] J. C.-W. Chan, J. Ma, and F. Canters, "A comparison of superresolution reconstruction methods for multi-angle CHRIS/PROBA images," *Proc. SPIE Remote Sens. Int. Soc. Opt. Photon.*, vol. 7109, pp. 710904-1–710904-11, Oct. 2008.
- [15] J. Ma and J. C.-W. Chan, "Superresolution reconstruction of hyperspectral remote sensing imagery using constrained optimization of POCS," in *Proc. IEEE Geosci. Remote Sens. Symp. (IGARSS)*, Jul. 2012, pp. 7271–7274.
- [16] H. Zhang, L. Zhang, and H. Shen, "A super-resolution reconstruction algorithm for hyperspectral images," *Signal Process.*, vol. 92, no. 9, pp. 2082–2096, 2012.
- [17] V. P. Shah, N. H. Younan, and R. L. King, "An efficient pan-sharpening method via a combined adaptive PCA approach and contourlets," *IEEE Trans. Geosci. Remote Sens.*, vol. 46, no. 5, pp. 1323–1335, May 2008.
- [18] S. Rahmani, M. Strait, D. Merkurjev, M. Moeller, and T. Wittman, "An adaptive IHS pan-sharpening method," *IEEE Geosci. Remote Sens. Lett.*, vol. 7, no. 4, pp. 746–750, Oct. 2010.
- [19] G. A. Licciardi, M. M. Khan, J. Chanussot, A. Montanvert, L. Condat, and C. Jutten, "Fusion of hyperspectral and panchromatic images using multiresolution analysis and nonlinear PCA band reduction," *EURASIP J. Adv. Signal Process.*, vol. 2012, no. 1, p. 207, 2012.
- [20] Y. Zhao, J. Yang, and J. C.-W. Chan, "Hyperspectral imagery super-resolution by spatial-spectral joint nonlocal similarity," *IEEE J. Sel. Topics Appl. Earth Observ. Remote Sens.*, vol. 7, no. 6, pp. 2671–2679, Jun. 2014.
- [21] X. X. Zhu and R. Bamler, "A sparse image fusion algorithm with application to pan-sharpening," *IEEE Trans. Geosci. Remote Sens.*, vol. 51, no. 5, pp. 2827–2836, May 2013.

- [22] J. Yang, J. Wright, T. S. Huang, and Y. Ma, "Image super-resolution via sparse representation," *IEEE Trans. Image Process.*, vol. 19, no. 11, pp. 2861–2873, Nov. 2010.
- [23] S. Wang, L. Zhang, Y. Liang, and Q. Pan, "Semi-coupled dictionary learning with applications to image super-resolution and photo-sketch synthesis," in *Proc. IEEE Conf. Comput. Vis. Pattern Recognit. (CVPR)*, Jun. 2012, pp. 2216–2223.
- [24] R. Gomez, A. Jazaeri, and M. Kafatos, "Wavelet-based hyperspectral and multi-spectral image fusion," *Aerospace/Defense Sens., Simul., Controls Int. Soc. Opt. Photon.*, vol. 4383, pp. 36–42, Jun. 2001.
- [25] R. C. Hardie, M. T. Eismann, and G. L. Wilson, "MAP estimation for hyperspectral image resolution enhancement using an auxiliary sensor," *IEEE Trans. Image Process.*, vol. 13, no. 9, pp. 1174–1184, Sep. 2004.
- [26] C. Grohfeldt, X. X. Zhu, and R. Bamler, "Jointly sparse fusion of hyperspectral and multispectral imagery," in *Proc. IEEE Conf. Geosci. Remote Sens. Symp. (IGARSS)*, Jul. 2013, pp. 4090–4093.
- [27] N. Yokoya, T. Yairi, and A. Iwasaki, "Coupled nonnegative matrix factorization unmixing for hyperspectral and multispectral data fusion," *IEEE Trans. Geosci. Remote Sens.*, vol. 50, no. 2, pp. 528–537, Feb. 2012.
- [28] J. M. Bioucas-Dias *et al.*, "Hyperspectral unmixing overview: Geometrical, statistical, and sparse regression-based approaches," *IEEE J. Sel. Topics Appl. Earth Observat. Remote Sens.*, vol. 5, no. 2, pp. 354–379, Apr. 2012.
- [29] M. Aharon, M. Elad, and A. Bruckstein, "K-SVD: An algorithm for designing overcomplete dictionaries for sparse representation," *IEEE Trans. Signal Process.*, vol. 54, no. 11, pp. 4311–4322, Nov. 2006.
- [30] W. Dong, L. Zhang, G. Shi, and X. Wu, "Image deblurring and super-resolution by adaptive sparse domain selection and adaptive regularization," *IEEE Trans. Image Process.*, vol. 20, no. 7, pp. 1838–1857, Jul. 2011.
- [31] D. L. Donoho, "For most large underdetermined systems of linear equations the minimal ℓ_1 -norm solution is also the sparsest solution," *Commun. Pure Appl. Math.*, vol. 59, no. 6, pp. 797–829, Jun. 2006.
- [32] L. Loncan *et al.*, "Hyperspectral pansharpening: A review," *IEEE Geosci. Remote Sens. Mag.*, vol. 3, no. 3, pp. 27–46, Sep. 2015.
- [33] N. Keshava and J. F. Mustard, "Spectral unmixing," *IEEE Signal Process. Mag.*, vol. 19, no. 1, pp. 44–57, Jan. 2002.
- [34] M.-D. Iordache, J. Bioucas-Dias, and A. Plaza, "Sparse unmixing of hyperspectral data," *IEEE Trans. Geosci. Remote Sens.*, vol. 49, no. 6, pp. 2014–2039, Jun. 2011.
- [35] M. V. Afonso, J. M. Bioucas-Dias, and M. A. T. Figueiredo, "An augmented Lagrangian approach to the constrained optimization formulation of imaging inverse problems," *IEEE Trans. Image Process.*, vol. 20, no. 3, pp. 681–695, Mar. 2011.
- [36] R. Rubinstein, M. Zibulevsky, and M. Elad, "Efficient implementation of the k -SVD algorithm using batch orthogonal matching pursuit," *Dept. Comput. Sci., Technion-Israel Inst. Technol., Tech. Rep.* 40, 2008.
- [37] A. Beck and M. Teboulle, "A fast iterative shrinkage-thresholding algorithm for linear inverse problems," *SIAM J. Imag. Sci.*, vol. 2, no. 1, pp. 183–202, 2009.
- [38] Z. Shi, Z. An, and Z. Jiang, "Hyperspectral image fusion by the similarity measure-based variational method," *Opt. Eng.*, vol. 50, no. 7, pp. 077006-1–077006-11, Jul. 2011.
- [39] D. C. Heinz and C.-I. Chang, "Fully constrained least squares linear spectral mixture analysis method for material quantification in hyperspectral imagery," *IEEE Trans. Geosci. Remote Sens.*, vol. 39, no. 3, pp. 529–545, Mar. 2001.
- [40] M.-D. Iordache, J. Bioucas-Dias, and A. Plaza, "Total variation spatial regularization for sparse hyperspectral unmixing," *IEEE Trans. Geosci. Remote Sens.*, vol. 50, no. 11, pp. 4484–4502, Nov. 2012.



Chen Yi received the B.S. and M.S. degrees in information engineering and control engineering from Northwestern Polytechnic University, Xi'an, China, in 2013 and 2016, respectively, where she is currently pursuing the Ph.D. degree with the School of Automation.

Her research interests include hyperspectral image processing.



Yong-Qiang Zhao

(M'05) received the B.S., M.S., and Ph.D. degrees in control science and engineering from Northwestern Polytechnic University, Xi'an, China, in 1998, 2001, and 2004, respectively.

From 2007 to 2009, he was a Post-Doctoral Researcher at McMaster University, Hamilton, ON, Canada, and Temple University, Philadelphia, PA, USA, respectively. He is currently a Professor with Northwestern Polytechnical University. His research interests include polarization vision, hyperspectral imaging, compressive sensing, and pattern



Jingxiang Yang (S'14) received the B.S. degree in automation from Anhui Polytechnic University, Wuhu, China, in 2011, and the M.S. degree in control theory and control engineering from Northwestern Polytechnic University, Xi'an, China, in 2014, where he is currently pursuing the Ph.D. degree with the School of Automation.

His research interests include hyperspectral image processing, sparse representation, and deep learning.



Jonathan Cheung-Wai Chan received the Ph.D. degree from the University of Hong Kong, Hong Kong, in 1999.

From 1998 to 2001, he was with the Department of Geography, University of Maryland, College Park, MD, USA. From 2001 to 2005, he was with the Interuniversity Micro-Electronics Centre, Leuven, Belgium. From 2005 to 2011, he was with the Department of Geography, Vrije Universiteit Brussel (VUB), Brussels, Belgium. From 2013 to 2014, he received a Marie Curie fellowship at Fondazione Edmund Mach, Trentino, Italy. He is currently a Senior Researcher and a Guest Professor with the Department of Electronics and Informatics, VUB. He is also a Visiting Professor with the Warsaw University of Life Sciences, Warsaw, Poland. His research interests include machine learning classification algorithms, hyperspectral remote sensing, and spatial enhancement of satellite hyperspectral images and their applications.

Dr. Chan is a Guest Editor of the *Remote Sensing* journal.



Seong G. Kong (SM'03) received the B.S. and M.S. degrees in electrical engineering from Seoul National University, Seoul, South Korea, in 1982 and 1987, respectively, and the Ph.D. degree in electrical engineering from the University of Southern California, Los Angeles, CA, USA, in 1991.

He was an Associate Professor of Electrical and Computer Engineering at the University of Tennessee, Knoxville, TN, USA, and Temple University, Philadelphia, PA, USA. He served as the Chair with the Department of Electrical Engineering, Soongsil University, Seoul, and the Graduate Program Director with the Electrical and Computer Engineering Department, Temple University. He is currently a Professor of Computer Engineering and the Director of Strategic Planning with Sejong University, Seoul. His research interests include image processing, computer vision, hyperspectral imaging, and intelligent systems.

Dr. Kong received the Honorable Mention Paper Award from the American Society of Agricultural and Biological Engineers in 2005 and the Most Cited Paper Award from the *Computer Vision and Image Understanding* journal in 2007 and 2008. He was an Associate Editor of the *IEEE TRANSACTIONS ON NEURAL NETWORKS* and a Guest Editor of the *Journal of Sensors*.